



Vibration amplitude mapping by stroboscopic structured light projection

I.L.F. Ribeiro^a, G.L. Carvalho^a, L.F.G. Dib^a, E.A. Barbosa^{a,b,*}, N.U. Wetter^c

^a Faculdade de Tecnologia de São Paulo, CEETEPS, São Paulo, Brazil

^b Centro Universitário da FEI, São Bernardo do Campo, Brazil

^c Centro de Lasers e Aplicações, IPEN/CNEN, São Paulo, Brazil

ARTICLE INFO

Keywords:

Structured light projection
Fringe evaluation
Stroboscopy
Vibration measurement

ABSTRACT

In this work a method to evaluate the distribution of vibration amplitudes of objects was demonstrated, combining for the first time oblique structured light projection, stroboscopic illumination and fringe evaluation. The light pattern was formed by straight and parallel fringes produced by a slightly misaligned Twyman–Green interferometer illuminated by a 40-mW, 650-nm diode laser. Stroboscopic illumination was achieved by driving the laser with a PWM signal with the same frequency than that of the vibrating object. By evaluating the fringes with phase stepping and phase unwrapping procedures, the amplitude mapping of a formica bar and circular rubber membranes was performed. By averaging the fringe position over the light pulse duration a correction ratio between the actual phase and the measured phase was obtained as a function of the pulse duty cycle, and the dependence of the fringe visibility on the duty cycle was studied. The experiments showed that relatively large amplitudes in a range from tens of millimeters up to few millimeters can be measured.

1. Introduction

It has been widely reported in the literature that optical methods are powerful tools for vibration measurement, many of them resulting in commercial devices for industrial applications. Optical techniques are distinguished from the conventional ones that use e.g. accelerometers mainly for providing non-contact testing, avoiding the influence of the measuring device over the object to be tested. Whole-field interferometric methods like time averaged holography [1] and time averaged speckle interferometry [2] have the advantage of being highly sensitive and precise. However, those techniques are limited to vibration amplitudes below the micrometer range, otherwise the resulting interferogram has a very poor visibility and an excessively high spatial frequency fringe pattern. Variations of these methods were developed in order to overcome those limitations, using stroboscopic illumination [3], phase-modulated reference beams [4,5] or double-pulse holography [6]. In all cases the fringe visibility can be somewhat increased and the dynamic range can be enlarged. Nevertheless, those variations cannot avoid the requirement of severe vibration isolation of the optical setup.

Laser Doppler vibrometry provides larger amplitude measurements and finds many [7] applications in industry [8], in medicine [9], in acoustics [10] and MEMS characterization [11] among many others. However, whole-field measurements [12,13] can only be performed by LDV by scanning the measured surface with a moving mirror.

For its remarkable simplicity, reliability and high reproducibility, structured light projection is by far the most used technique for surface shaping and has innumerable applications in several fields such as dentistry [14], medicine [15,16], facial recognition [17], reverse engineering [18,19] and historical restoration [20], among others. Nevertheless, structured light is less commonly used in displacement measurement and dynamical process testing. Works on this field report different forms to compensate for the loss of light pattern visibility due to the surface vibration. In reference [21] a sequence of fringe patterns generated by a moving grating and acquired by a high-speed camera was used to analyze the vibration of a vibrating bar; the vibration map of an Aluminum cantilever was studied with the help of Talbot fringes generated by a Ronchi grating and analyzed by Fourier transform [22]; structured light with vertical and horizontal fringes from a He–Ne with a core fiber did enable to map vibration amplitudes of flat surfaces by obtaining the amplitude distribution from the inverse of the zeroth-order Bessel function [23] and a high-speed camera was used to capture images of a drumhead illuminated by a sinusoidal light pattern [24]; the visibility decrease of projected fringe patterns produced by vibrating surfaces was studied for vibration amplitude mapping [25].

In our work the structured light formed of straight and parallel interference fringes was produced by a Twyman–Green interferometer illuminated by a red diode laser. In order to get a static light pattern projected onto the surface we used stroboscopic illumination by driving the laser with a PWM (pulse width modulated) signal with the same frequency of the object vibration. The amplitude mapping was carried

* Corresponding author at: Faculdade de Tecnologia de São Paulo, CEETEPS, São Paulo, Brazil.

E-mail address: ebarbosa@fatecsp.br (E.A. Barbosa).

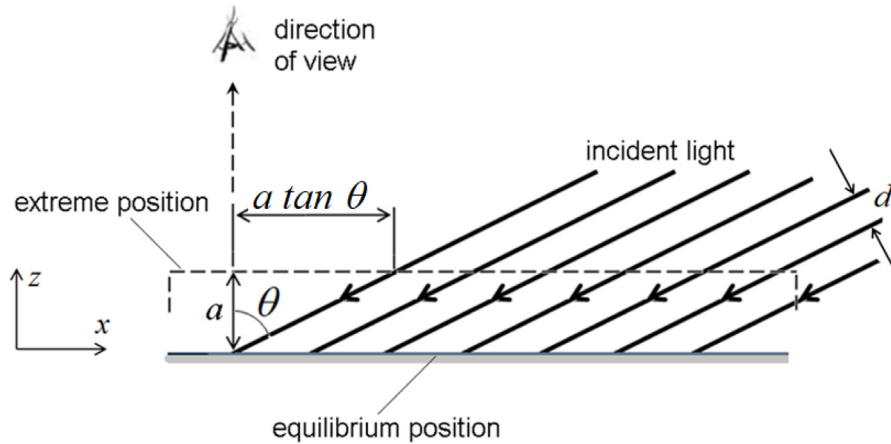


Fig. 1. Fringe projection onto the vibrating surface.

out through the four stepping technique [26] and the resulting phase was unwrapped by the branch-cut method [27]. We obtained the vibration amplitude mapping of a $20 \times 90 \text{ mm}^2$ formica bar and of 51-mm diameter rubber membranes of different thicknesses and measured vibration amplitudes of up to 2.05 mm.

This article is organized as follows: in Section 2 the fringe projection, the stroboscopic illumination process and the fringe evaluation procedures are described, as well as the influence of the duty cycle on the fringe visibility and the averaged phase are analyzed; Section 3 describes the experimental setup and procedure; in Section 4 the results are presented and discussed and the concluding remarks are presented in Section 5.

2. Fringe pattern incidence onto a vibrating surface

Consider a flat surface parallel to plane xy harmonically vibrating along the z -axis with frequency and amplitude a and illuminated by a uniform fringe pattern represented by the parallel arrows shown in Fig. 1. The fringes are observed along the z -axis. If the angle of incidence is θ , a fringe projected on the surface and observed along the z direction undergoes a maximum lateral displacement $\Delta x_{max} = a \tan\theta$. Hence, a given bright or dark fringe will oscillate in time according to $x(t) = a \tan\theta \cos(\omega t)$. If the frequency is sufficiently higher than the optical acquisition rate the resulting light pattern appears completely blurred or undergoes a visibility decrease.

Consider now that the incident light is amplitude modulated according to a time-modulated PWM function $F(\Omega, t, \phi)$, where Ω is the signal frequency and ϕ is the phase with respect to the surface vibration. When this light illuminates the oscillating surface, the position of the projected fringe pattern is then given by

$$x(t) = a \tan\theta \cos(\omega t) F(\Omega, t, \phi) \quad (1)$$

The value of Ω can be set such that the frequency of the vibrating object and the diode laser are equal and the projected light pattern on the surface appears to be static. In order to enhance the resulting interferogram visibility the light duty cycle must be properly set. The value of ϕ determines the position in which the vibrating object is illuminated.

2.1. Four stepping procedure

Once a good visibility and static interferogram is obtained, the procedure for amplitude mapping is essentially the same as for surface contouring by fringe projection. As will be seen in the next subsection,

the fringe pattern frozen by the stroboscopic illumination is given as a function of the fringe visibility m and the average phase $\langle \phi_{ob} \rangle$ as

$$I(x, t) = \frac{I_0}{2} + \frac{I_0 m \cos(kx + \langle \phi_{ob} \rangle + \phi_{PZT})}{2} \quad (2)$$

where k is the light pattern spatial frequency, I_0 is the maximal light intensity and ϕ_{PZT} is the phase applied on the fringe pattern for phase stepping.

The wrapped phase $\Phi = kx + \langle \phi_{ob} \rangle$ describing the object shape can be determined by the four-stepping procedure by acquiring four sequentially -shifted interferograms with intensities I_1, I_2, I_3 and I_4 to get [16,28]

$$\phi_{ob} = \arctan\left(\frac{I_4 - I_2}{I_1 - I_3}\right) - kx \quad (3)$$

By applying phase unwrapping methods described elsewhere [17, 29] the phase is unwrapped in 256 gray levels, ranging from 0 (black) to 255 (white), which allows determining the object shape in its maximum displacement. The same procedure is carried out again to obtain the object shape at its equilibrium position (without vibration) as

$$\phi'_{ob} = \arctan\left(\frac{I_4 - I_2}{I_1 - I_3}\right) - kx \quad (4)$$

where I_i , is the light intensity of the i th frame of the static object. Hence, the object shape due to the vibration is simply determined from Eqs. (2) and (3) as

$$\Delta\phi_{ob} = \phi_{ob} - \phi'_{ob} \quad (5)$$

By converting $\Delta\phi_{ob}$ into amplitude coordinates one obtains the amplitude distribution along the studied surface. It should be emphasized that the term ϕ_{ob} is the average of the object phase taken along the PWM pulse duration, as will be seen in the next section.

2.2. Averaged phase and visibility of the fringe pattern in the stroboscopic regime

It is worth evaluating the dependence of the illuminating pattern phase and visibility on the duty cycle of the pulsed light, i.e., the ratio between the pulsed duration Δt and the period T of the PWM signal, in order to enhance the measurement accuracy and to establish the best experimental parameters for stroboscopic illumination.

Consider that the surface vibrates in an out-of-plane fashion with frequency ω and temporal arbitrary phase ϕ along the z -axis with amplitude a according to $z(t) = a \sin(\omega t + \phi)$. The light pattern oscillates

with amplitude $a \tan\theta$ along the x -axis according to $a \tan\theta \sin(\omega t + \varphi)$, and the pattern is viewed along the z direction according to [25]

$$I(x, t) = \frac{I_0}{2} + \frac{I_0}{2} \cos \left[\frac{2\pi}{d} \cos\theta x - \frac{2\pi}{d} a \sin\theta \sin(\omega t + \varphi) \right] \quad (6)$$

where d is the pattern spatial period (see Fig. 1). Under stroboscopic illumination, the intensity of the observed pattern is obtained upon averaging Eq. (6) in the vibration period and considering that the object is illuminated during the pulse:

$$\begin{aligned} \langle I(x) \rangle &= \frac{1}{T} \int_{t-\Delta t/2}^{t+\Delta t/2} \frac{I_0}{2} dt + \frac{I_0}{2} \cos(kx) \frac{1}{T} \int_{t-\Delta t/2}^{t+\Delta t/2} \cos[\phi_{ob} \sin(\omega t' + \varphi)] dt' \\ &+ \frac{I_0}{2} \sin(kx) \frac{1}{T} \int_{t-\Delta t/2}^{t+\Delta t/2} \sin[\phi_{ob} \sin(\omega t' + \varphi)] dt' \end{aligned} \quad (7)$$

where $\phi_{ob} \equiv 2\pi a \sin\theta/d$ and the pattern spatial frequency is $k \equiv 2\pi \cos\theta/d$. It is of our interest to register the extreme object position, which corresponds to the minimal or maximal x -position of the interference pattern viewed by the observer along the z -axis in Fig. 1. Hence, by conveniently setting $\varphi = 0$, one gets for the minimal or maximal position $\omega t = \pm(N + 1/2)\pi$, $N = 0, 1, 2, 3, \dots$, and the integrals of Eq. (7) are calculated at $t = (N + 1/2)T/2$. By writing the pulse duration as $\Delta t = \eta T$, where η is the duty cycle, the time averaged fringe pattern becomes

$$\begin{aligned} \langle I(x) \rangle &= \eta \frac{I_0}{2} + \frac{I_0}{2} \cos(kx) \left[\eta J_0(\phi_{ob}) + 2\eta \sum_{n=1}^{\infty} (-1)^n J_{2n}(\phi_{ob}) \operatorname{sinc}(2\pi n\eta) \right] \\ &+ \frac{I_0}{2} \sin(kx) 2\eta \sum_{n=1}^{\infty} (-1)^{n-1} J_{2n-1}(\phi_{ob}) \operatorname{sinc}[(2n-1)\pi\eta] \end{aligned} \quad (8)$$

where J_i is the i th order Bessel function of the first kind. Eq. (8) was obtained with the help of the identities

$$\cos[\phi_{ob} \sin(\omega t)] = J_0(\phi_{ob}) + 2 \sum_{n=1}^{\infty} J_{2n}(\phi_{ob}) \cos[2n\omega t]$$

$$\sin[\phi_{ob} \sin(\omega t)] = 2 \sum_{n=1}^{\infty} J_{2n-1}(\phi_{ob}) \sin[(2n-1)\omega t]$$

As an example, Fig. 2a simulates the intensity profile of a \cos^2 fringe pattern projected onto a vibrating flat surface averaged over a PWM signal with the (unrealistically small) duty cycle of $\eta = 0.01$, for $\phi_{ob} = 1.8$ rad. The thick dark function is the static pattern in the equilibrium position, while the dotted function is the averaged curve, both obtained from Eq. (8). Fig. 2b compares the equilibrium pattern (dark curve) with the averaged intensity (dotted curve) for $\eta = 0.4$ and the same value of ϕ_{ob} . Fig. 2c in turn shows the same comparison for $\eta = 0.6$. Fig. 2a, b and c have the same vertical and horizontal scales. Notice that as the duty cycle increases the pattern visibility decreases, since the difference between the maxima and the minima of the dotted patterns progressively diminishes. It can also be noticed that the maximal phase difference between the equilibrium and the displaced patterns decreases with the duty cycle increase, i.e., the average maximum fringe displacement depends on the duty cycle and is smaller than the actual maximum value of ϕ_{ob} . This is due to the fact that the finite pulse width of the PWM signal makes the fringe pattern to be continuously registered in the time intervals before $(t - \Delta t/2)$ and after $(t + \Delta t/2)$ the fringe pattern reaches its maximum displacement. In Fig. 2, all the dotted curves were multiplied by $1/\eta$ in order to ease visualization and comparison.

The average phase $\langle \phi_{ob} \rangle$ due to the surface vibration during the pulse is determined considering that Eq. (8) in the stroboscopic regime must have the form

$$\langle I(x) \rangle = \eta \left[\frac{I_0}{2} + \frac{I_0}{2} m \cos(kx - \langle \phi_{ob} \rangle) \right] \quad (9)$$

By combining Eqs. (8) and (9) one gets

$$\langle \phi_{ob} \rangle = \arctan \left\{ \frac{2 \sum_{n=1}^{\infty} (-1)^{n-1} J_{2n-1}(\phi_{ob}) \operatorname{sinc}[(2n-1)\pi\eta]}{J_0(\phi_{ob}) + 2 \sum_{n=1}^{\infty} (-1)^n J_{2n}(\phi_{ob}) \operatorname{sinc}(2\pi n\eta)} \right\} \quad (10)$$

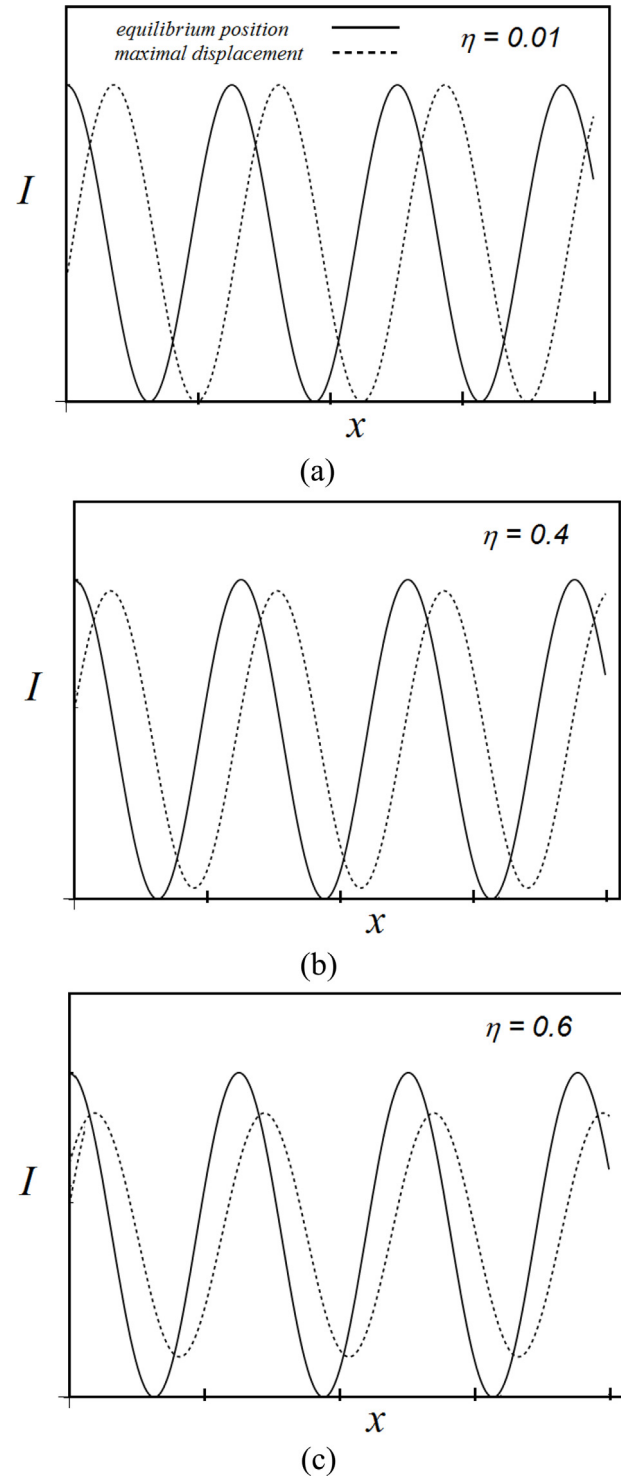


Fig. 2. Intensity profile of the light pattern projected onto a flat surface in its equilibrium position (dark curve) and average of the light pattern in its extreme position (dotted curve) for a - $\eta = 0.01$; b - $\eta = 0.4$; c - $\eta = 0.6$.

Fig. 3 displays the ratio $\langle \phi_{ob} \rangle / \phi_{ob}$ as a function of the duty cycle η calculated from Eq. (10). This relationship may be regarded as a correction ratio through which the real value ϕ_{ob} is determined from the measured phase $\langle \phi_{ob} \rangle$ depending on η , thus enabling more accurate

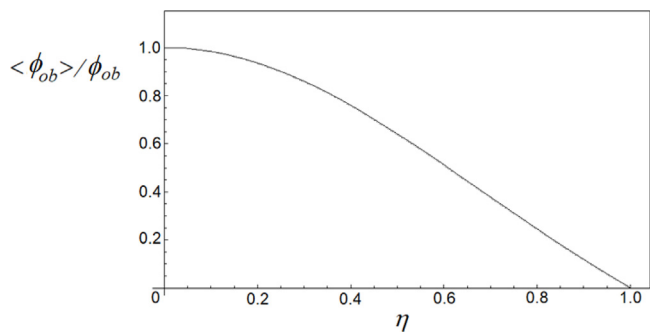


Fig. 3. Ratio between the average phase $\langle \phi_{ob} \rangle$ and the actual phase ϕ_{ob} as a function of the duty cycle.

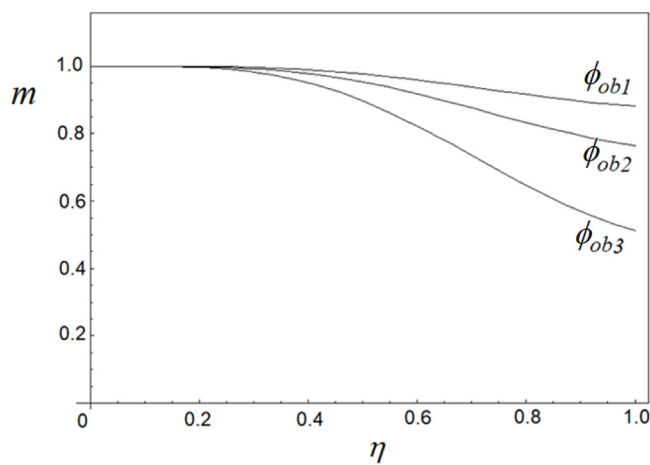


Fig. 4. Visibility of the fringe pattern as a function of the duty cycle η for $\phi_{ob1} = 0.7$ rad, $\phi_{ob2} = 1.0$ rad and $\phi_{ob3} = 1.5$ rad.

measurements. As expected, larger values of η imply smaller phase averages, and $\langle \phi_{ob} \rangle \rightarrow \phi_{ob}$ as $\eta \rightarrow 0$, at the cost of very low overall light intensities.

The visibility of the fringe pattern is also an important experimental parameter, since larger values of the fringe visibility m lead to measurements more immune to optical and electronic noise. From Eqs. (8) and (9) one can also obtain the dependence of the m on the duty cycle η , being m defined by $m = (I_{max} - I_{min}) / (I_{max} + I_{min})$, where I_{max} and I_{min} are the intensities of the interference maxima and minima, respectively:

$$m = \frac{J_0(\phi_{ob}) + 2 \sum_{n=1}^{\infty} (-1)^n J_{2n}(\phi_{ob}) \text{sinc}(2\pi n \eta)}{\cos \langle \phi_{ob} \rangle} = \frac{2 \sum_{n=1}^{\infty} (-1)^{n-1} J_{2n-1}(\phi_{ob}) \text{sinc}[(2n-1)\pi \eta]}{\sin \langle \phi_{ob} \rangle} \quad (11)$$

The dependence of the visibility on the duty cycle is shown in Fig. 4 for three values of phase ϕ_{ob} , namely, 0.7, 1.0 and 1.5 rad, calculated from Eq. (11). The values of $\langle \phi_{ob} \rangle$ were determined from Eq. (10).

The results of Fig. 4 are useful as a guide for choosing a proper value of the duty cycle without significantly decreasing the pattern visibility. It is shown that in the approximate interval $0.2 < \eta < 0.3$ the visibility is just slightly decreased regardless the phase ϕ_{ob} with a proper overall light intensity.

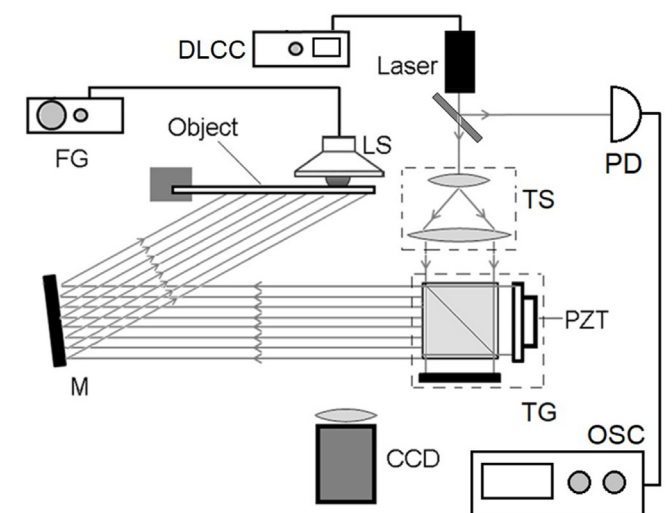


Fig. 5. Optical setup: TG, Twyman–Green interferometer; PZT, mirror attached to a piezo transducer; FG, function generator; DLCC, diode laser current driver; LS, loudspeaker; M, mirror; TS, telescope; CCD, camera; OSC, oscilloscope, PD, photodetector.

3. Experiments

The optical setup is shown in Fig. 5. The beam of a 40-mW red diode laser emitting at 653 nm is driven by a PWM signal with the help of a diode laser current controller DLCC (Thorlabs, LDC 205C) shown in the figure and is expanded and collimated by the telescope TS to illuminate the Twyman–Green interferometer TG. The light pattern formed by straight and parallel fringes (represented by the arrows in Fig. 5) emerging from the TG is deviated by mirror M and obliquely impinges the object surface. The objects are a $20 \times 90 \text{ mm}^2$ formica bar excited by the core of the woofer loudspeaker LS and is clamped at one end and two 51-mm diameter rubber membranes with different thicknesses, both clamped at their ends by metallic rings and excited at their centers by the LS. The incidence angle (see Fig. 1) onto the surface is $\theta = 70^\circ$. The object image is formed by a 640-lines CCD camera and is displayed and processed by a computer.

Both the LS and the diode laser are driven by independent signals. During the measurement procedure, as the object vibrates with frequency ω , the laser switching frequency Ω is continuously varied and as their values get closer, one observes the projected fringes oscillate back and forth with a beat frequency $|\omega - \Omega|$. Stroboscopic illumination is achieved by properly matching the frequencies (setting $= \Omega$) of both sources and by properly setting the value of their relative phases. This is carried out with the help of the beam partially deviated by the beam splitter BS and collected by the photodetector PD. The oscilloscope OSC displays both the signals originated from the PD and the laser driven signal. The PZT mirror of the TG is supported by a piezoelectric transducer in order to apply DC displacements and perform four stepping.

We opted to modulate the illuminating light with a duty cycle of 0.2, which was a good trade-off of visibility and overall intensity. The eventually relatively low pattern visibility is canceled out in the four stepping process, as predictable from Eq. (2). Moreover, in our experiments the vibrating surface was only illuminated at its highest position, were the velocity and the displacements are lowest, which enables more tolerant duty cycle choices without significantly decreasing the fringe visibility.

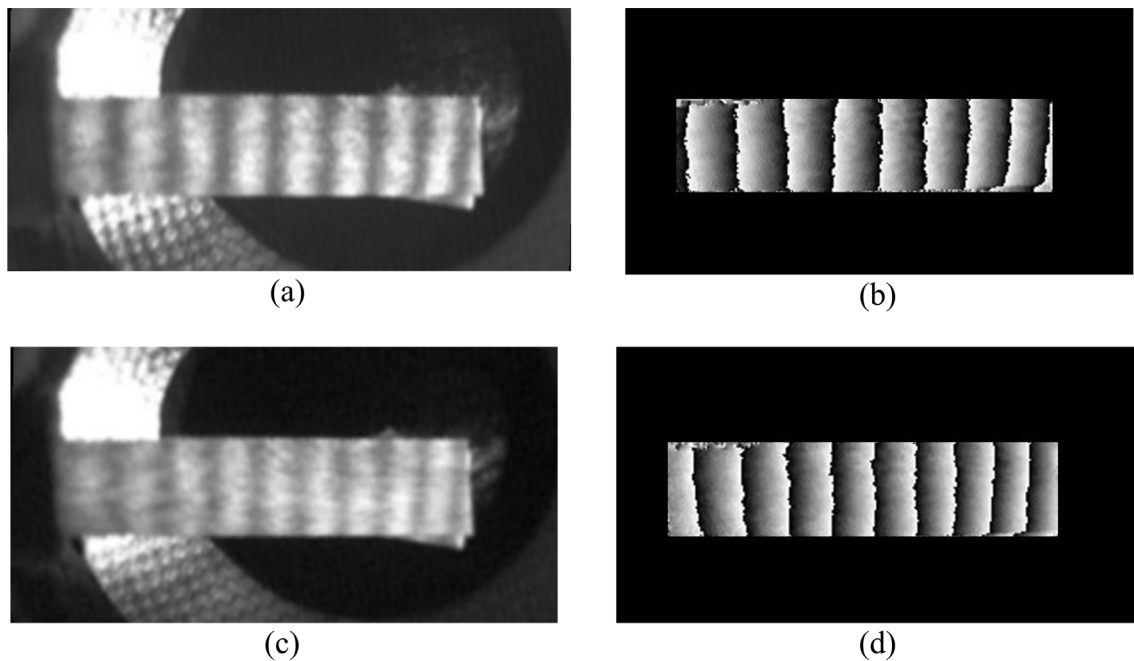


Fig. 6. a – Static bar illuminated by the fringe pattern; b – phase map of the static bar; c – Vibrating bar illuminated by the stroboscopic fringe pattern; d – phase map of the vibrating bar in its maximal deformation.

4. Results and discussion

4.1. Formica bar

Fig. 6a and b show the projected fringe pattern onto the static bar and the resulting phase map upon applying the four stepping procedure, respectively, while Fig. 6c and d show the fringe pattern and the phase map projected onto the formica plate vibrating at 54 Hz in the stroboscopic regime, for $\eta = 0.2$. According to Eq. (10) and Fig. 3, this value of η leads to the ratio $\langle \phi_{ob} \rangle / \phi_{ob} \approx 0.93$. The static bar is parallel to the CCD target, i.e., it is perpendicular to the optical axis. It can be noticed that the stroboscopic fringe pattern slightly reduces the fringe visibility, as predicted by Eq. (11) and shown in Fig. 4. The overall intensities of Fig. 6a and c are nearly the same due to the automatic adjustment of the CCD camera. By comparing both the fringe patterns and the phase maps one sees a larger concentration of fringes in the stroboscopic pattern, confirming that the bar was deformed in the vibration state with respect to its static state. Notice also that despite the slightly lower visibility of the stroboscopic fringe pattern, the phase maps of Fig. 6b and d have similarly low noise levels, in accordance with Eq. (2). The interferogram generated by the TG with nearly straight parallel fringes with spatial period 1.82 mm. Hence, after the four stepping and phase unwrapping the bar appears to be pseudo-tilted with respect to the CCD camera with planes of constant elevation of 1.82 mm.

Fig. 7 shows the z -coordinates of both the static ($z(x,y)$, white circles) and vibration ($Z(x,y)$, black squares) states of the bar taken along the horizontal x -axis in the middle of the bar after applying the unwrapping procedure. Fig. 8a shows the vibration amplitude map of the formica bar, after subtracting the bar shapes obtained in the vibrating and in the static mode, according to Eq. (5), while Fig. 8b shows the 3D reconstruction of the vibration amplitude distributed along the bar surface.

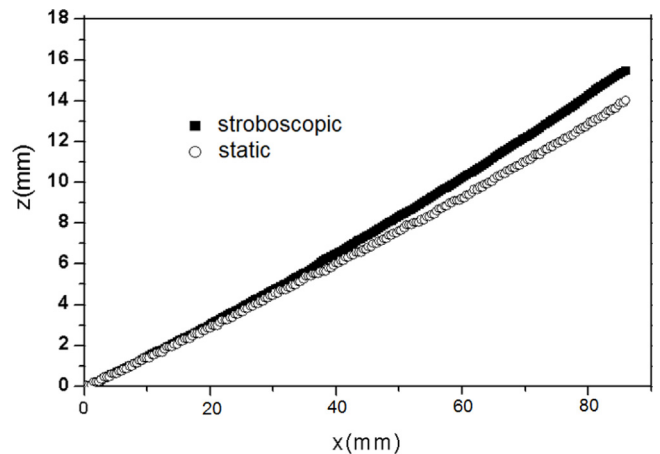


Fig. 7. z -coordinates of the pseudo-tilted static bar (white circles) and of the vibrating bar (black squares) taken along the horizontal x -axis.

4.2. Circular membrane

The 0.5-mm thick rubber membrane 1 illuminated by the fringe pattern in its static configuration is shown in Fig. 9a, while Fig. 9b shows the same membrane vibrating at 52.5 Hz and illuminated by the fringe pattern modulated at the same frequency with $\eta = 0.2$, so that $\langle \phi_{ob} \rangle / \phi_{ob} \approx 0.93$ again. The fringes were frozen by the stroboscopic illumination in their maximum displacement with respect to their static position. As performed in the previous section, the pseudo-tilted membrane shape in the static and in the stroboscopic configurations were retrieved by phase stepping and phase unwrapping, and the membrane amplitude distribution was then obtained with the help of Eq. (5). The

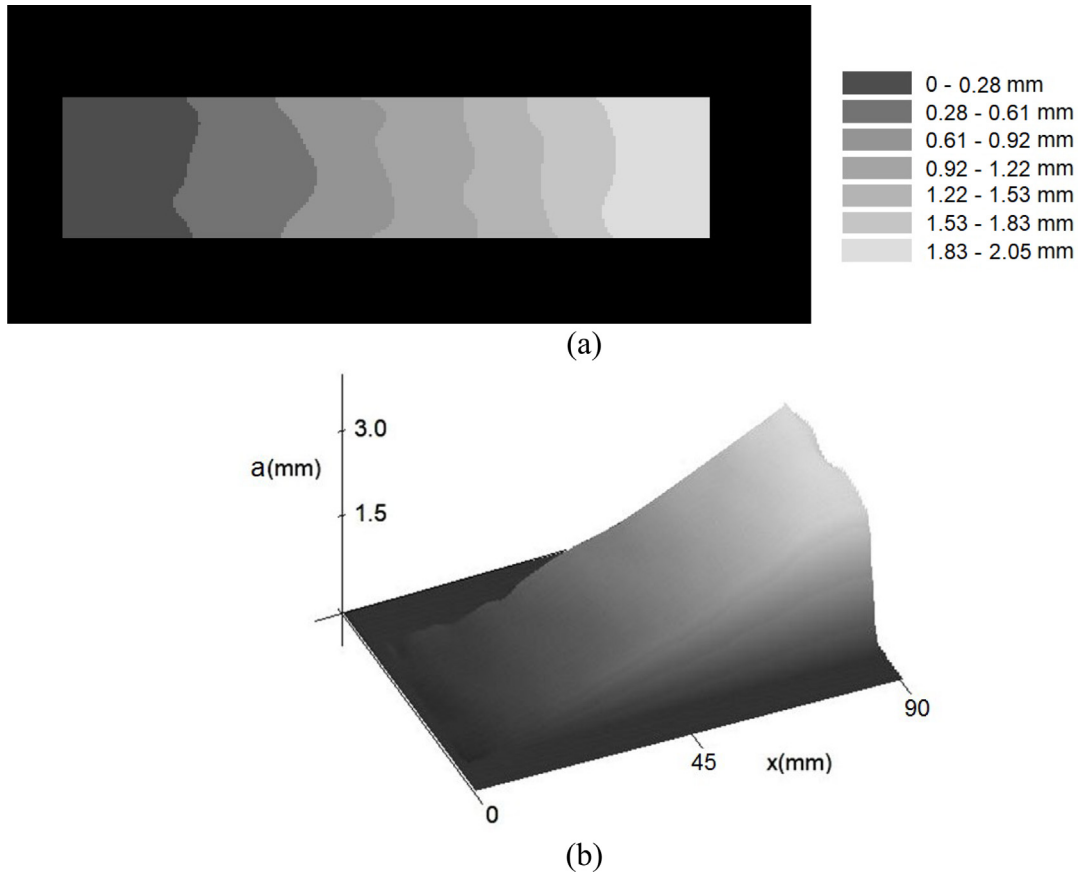


Fig. 8. a – Vibration amplitude map and b – 3D reconstruction of the vibration amplitude of the formica bar.

chart on the right of Fig. 9c shows the vibration amplitude values of each region on the membrane and Fig. 9d depicts the 3D reconstructed amplitude map, where the insert on the upper part of the figure shows the amplitude taken along the line parallel to the x direction through the center of the membrane.

The results of membrane 2 with the same diameter and with thickness 0.2 mm vibrating at 64.0 Hz are shown in Fig. 10. Fig. 10a shows the deformed projected fringe pattern due to the vibration and frozen by the stroboscopic illumination with $\eta = 0.2$, Fig. 10b shows the vibration amplitude map and Fig. 10c shows the 3D reconstructed amplitude map, with the upper insert showing the amplitude profile along the horizontal center line.

We estimate the potential sensitivity of the method. If the minimal observable phase shift of the fringe pattern is $\phi_{obmin} = \epsilon 2\pi$, where $0 < \epsilon < 1$, from the definition of ϕ_{ob} given in Section 2.2 one gets the minimal measurable amplitude as $a_{min} = \epsilon d / \sin\theta$, d and θ shown in Fig. 1. Let us arbitrarily and conservatively assume that the displacement of 1/5th of a fringe can be easily observed, i.e., $\epsilon = 0.2$ and that $\theta = 70^\circ$ as in the experimental setup. Hence, the minimal measurable surface displacement is $a_{min} \cong 0.2d$ in typical experimental conditions. This result shows that the minimum measurable amplitude can be decreased by scaling down the values of the light pattern spatial period, which is limited to the camera resolution. This limitation can be partially overcome by enlarging the magnification of the imaging system to provide more pixels per fringe, not without the expense of the size of the analyzed region. It is also recommended to use the smallest possible value of the duty cycle in order to achieve the highest possible sensitivity, since $\langle \phi_{ob} \rangle / \phi_{ob} \rightarrow 1$ in this case. Under such conditions and assuming that the spatial period of the pattern

projected onto the surface is of the order of few millimeters, the minimal measurable amplitude is determined to be of the order of few hundreds of micrometers.

From the phase $\phi_{ob} = 2\pi a \sin\theta / d$ defined in Section 2.2 it is possible to estimate the measurement uncertainty. From this relation and with the help of Fig. 1 one concludes that if the surface displacement along the z -axis is $H = d / \sin\theta$ the fringe pattern is displaced by one period, i.e., by regarding the fringe pattern as describing a pseudo-tilted surface the length H is the distance between two adjacent planes of constant elevation. In the experiments it can be accurately and precisely measured by imaging the fringe pattern generated by a planar object parallel to the xy -plane and supported by a translator displaced by a micrometric screw. Alternatively, it can be also indirectly made by translating mirror M of Fig. 5. By displacing three or four periods of the order of some millimeters with a 0.01-mm precision translator this previous calibration provides relative uncertainties typically of the order of $\delta H / H \cong 5 \times 10^{-3}$. The frames obtained in this work were obtained with 640 horizontal pixels; taking into account not only the pixel size but also factors like optical and electronic noise the phase relative uncertainty can be conservatively estimated to be $\delta \phi_{ob} / \phi_{ob} \cong 4 \times 10^{-3}$. Hence, one gets the relative uncertainty of the amplitude vibration as $\delta a / a = \sqrt{(\delta H / H)^2 + (\delta \phi_{ob} / \phi_{ob})^2} \cong 6 \times 10^{-3}$. The simplicity of both the relation $a = \phi_{ob} H / 2\pi$ and the measurement process may also provide very accurate results.

5. Conclusion

A method for measuring the vibration of surfaces with stroboscopic structured light projection was proposed and the amplitude mapping

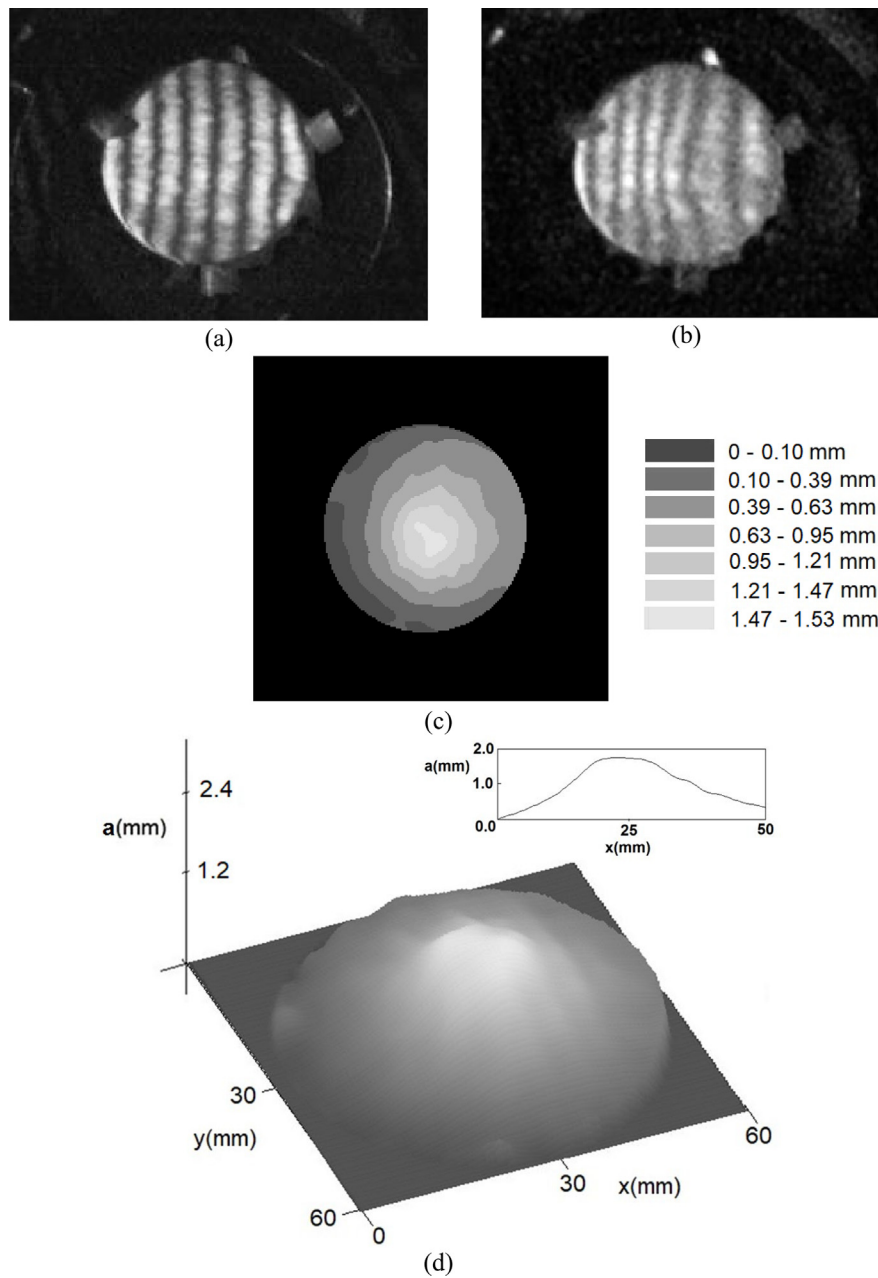


Fig. 9. a – Static membrane 1 illuminated by the fringe pattern; b – membrane 1 vibrating at 52.5 Hz stroboscopically illuminated with $\eta = 0.2$; c – vibration amplitude map; d – 3D reconstruction of the vibration amplitude of the membrane.

of objects of tens of cm^2 -area was demonstrated. The major original contribution of our work is combining for the first time three techniques of optical measurement methods that have previously been used in other works but not in this combination. These are structured light projection, stroboscopic illumination and phase stepping procedures, used to obtain the 3D reconstruction of the vibration amplitude distribution. Our method not only provides quantitative evaluation but also analysis by visual inspection. By sweeping the laser pulse frequency in the region near the object frequency the projected fringes oscillate back and forth with a beat frequency which can be made small enough in order to enable visualizing this fringe oscillation.

According to Eq. (5) the fact that the amplitude spatial distribution is determined from the difference between the phases of the vibration and the static states implies that our method allows the vibration study

not only of flat or nearly flat surfaces but also of objects with more complex geometries. In this case, it should be taken into account that the proposed method is capable of measuring the vibration component parallel to the viewing direction only.

The relation between the duty cycle, the measurement sensitivity and the fringe visibility was studied. Those results allow defining the best experimental conditions to reduce optical noise and optimizing measurement accuracy as well. It was shown that the method requires a very simple setup to provide a measurement range from tenths of millimeters up to several centimeters, which is usually not covered by speckle or holographic time averaged interferometry. In the present work the fringes were generated by a Twyman–Green interferometer, but the light pattern can also be originated from amplitude modulated low-coherence light sources. Those results point out to

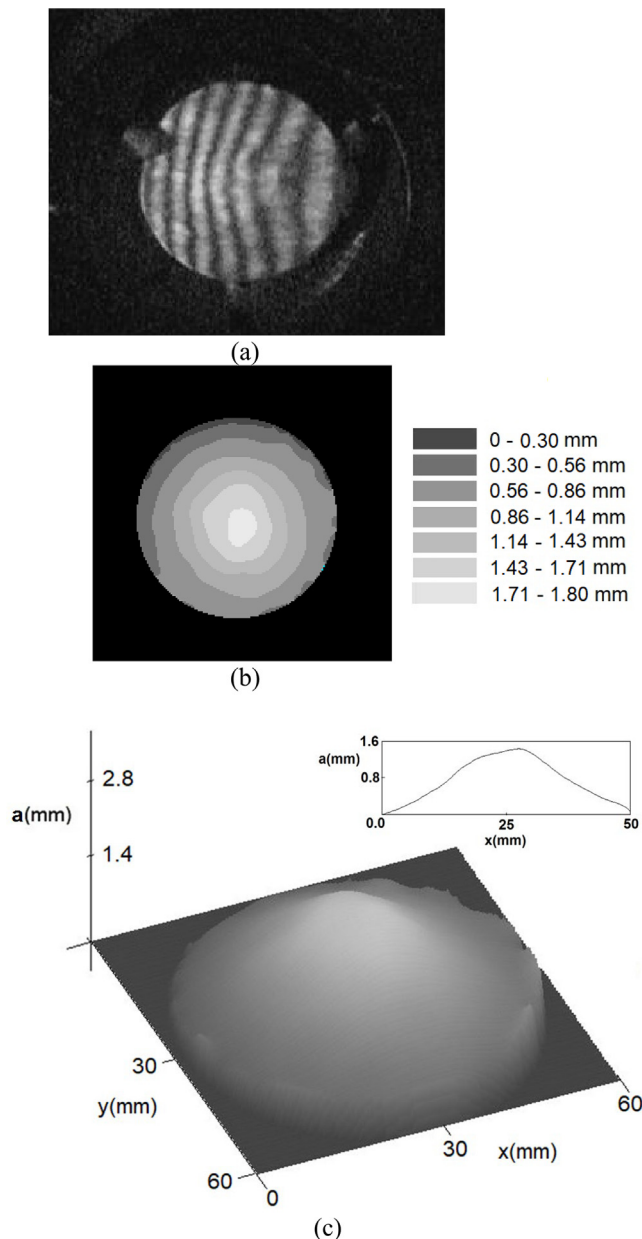


Fig. 10. a – Static membrane 2 illuminated by the fringe pattern; b – membrane 2 vibrating at 52.5 Hz stroboscopically illuminated with $\eta = 0.2$; c – vibration amplitude map; d – 3D reconstruction of the vibration amplitude of the membrane.

developing rugged and compact optical devices which can be operated in industrial, noisy environments.

Declaration of competing interest

The authors declare that they have no known competing financial interests or personal relationships that could have appeared to influence the work reported in this paper.

Data availability

No data was used for the research described in the article.

Acknowledgments

G. Carvalho received a scholarship from CNPq (Conselho Nacional de Pesquisa e Desenvolvimento), Brazil under Grant 103693/2022-0.

References

- [1] M. Stipčević, N. Demoli, H. Skenderović, M. Lončarić, A. Radman, J. Gladić, D. Lovrić, Effective procedure for determination of unknown vibration frequency and phase using time-averaged digital holography, *Opt. Express* 25 (9) (2017) 10241, <http://dx.doi.org/10.1364/OE.25.010241>.
- [2] B. Deepan, C. Quan, C.J. Tay, Quantitative vibration analysis using a single fringe pattern in time-average speckle interferometry, *Appl. Opt.* 55 (22) (2016) 5876, <http://dx.doi.org/10.1364/AO.55.005876>.
- [3] F. Verpillat, F. Joud, M. Atlan, M. Gross, Imaging velocities of a vibrating object by stroboscopic sideband holography, *Opt. Express* 20 (20) (2012) 22860, <http://dx.doi.org/10.1364/OE.20.022860>.
- [4] E.A. Barbosa, M. Muramatsu, Mapping of vibration amplitudes by time average holography in $\text{Bi}_{12}\text{SiO}_{20}$ crystals, *Opt. Las. Technol.* 29 (7) (1997) 359, [http://dx.doi.org/10.1016/S0030-3992\(97\)00041-8](http://dx.doi.org/10.1016/S0030-3992(97)00041-8).
- [5] Ole J. Løkberg, Kåre Høgmoen, Vibration phase mapping using electronic speckle pattern interferometry, *Appl. Opt.* 15 (11) (1976) 2701, <http://dx.doi.org/10.1364/AO.15.002701>.
- [6] G. Pedrini, S. Schedin, H.J. Tiziani, Pulsed digital holography combined with laser vibrometry for 3D measurements of vibrating objects, *Opt. Las. Eng.* 38 (3) (2002) 117, [http://dx.doi.org/10.1016/S0143-8166\(02\)00005-2](http://dx.doi.org/10.1016/S0143-8166(02)00005-2).
- [7] F. Baldini, C.I. Moir, J. Homola, R.A. Lieberman, Miniature laser doppler velocimetry systems, in: Francesco Baldini, Jiri Homola, Robert A. Lieberman (Eds.), *Optical Sensors*, 2009, p. 12, <http://dx.doi.org/10.1117/12.819324>.
- [8] N.K. Pachisia, K. Tiwari, R. Das, Multiple reflection assisted Laser Doppler vibrometer setup for high resolution displacement measurement, *Opt. Commun.* 464 (2021) 125504, <http://dx.doi.org/10.1016/j.optcom.2020.125504>.
- [9] A.M. Huber, C. Schwab, T. Linder, S.J. Stoeckli, M. Ferrazzini, N. Dillier, U. Fisch, Evaluation of eardrum laser doppler interferometry as a diagnostic tool, *Laryngoscope* 111 (3) (2001) 501, <http://dx.doi.org/10.1097/00005537-200103000-00022>.
- [10] K. Yuan, W.D. Zhu, A novel general-purpose three-dimensional continuously scanning laser Doppler vibrometer system for full-field vibration measurement of a structure with a curved surface, *J. Sound Vib.* 540 (2022) 117274, <http://dx.doi.org/10.1016/j.jsv.2022.117274>.
- [11] C. Rembe, G. Siegmund, H. Steger, M. Wörtge, *Measuring MEMS in motion by laser Doppler vibrometry*, in: Wolfgang Osten (Ed.), *Optical Inspection of Microsystems*, Taylor and Francis, 2018.
- [12] A.R. Harland, J.N. Petzing, J.R. Tyrer, Nonperturbing measurements of spatially distributed underwater acoustic fields using a scanning laser Doppler vibrometer, *J. Acoust. Soc. Am.* 115 (1) (2004) <http://dx.doi.org/10.1121/1.1635841>.
- [13] G.R. Ball, A. Huber, R.L. Goode, Scanning laser Doppler vibrometry of the middle ear ossicles, *Ear Nose Throat J.* 76 (4) (1997) 213.
- [14] J. Geng, Three-dimensional dental imaging method and apparatus having a reflective member, 2003, U.S. patent 6, 594, 539.
- [15] C. Schmalz, F. Forster, A. Schick, E. Angelopoulou, An endoscopic 3D scanner based on structured light, *Med. Image Anal.* 16 (5) (2012) 1063, <http://dx.doi.org/10.1016/j.media.2012.04.001>.
- [16] H.-T. Change, C.H. Wang, S.-S. Lee, W.-J. Wu, C.-K. Lee, Continuous measurement of wrist artery pulse vibration signals using structured-light projection method, in: Proceedings of SPIE 11352, Optics and Photonics for Advanced Dimensional Metrology, Spie Photonics Europe, 2020, 1135211, <http://dx.doi.org/10.1117/12.2555341>.
- [17] C.L. Heike, K. Upson, E. Stuhau, S.M. Weinberg, 3D digital stereophotogrammetry: a practical guide to facial image acquisition, *Head Face Med.* 6 (1) (2010) 18, <http://dx.doi.org/10.1186/1746-160X-6-18>.
- [18] X. Zexiao, W. Jianguo, Z. Qiumei, Complete 3D measurement in reverse engineering using a multi-probe system, *Int. J. Mach. Tools Manuf.* 45 (12–13) (2005) 1474, <http://dx.doi.org/10.1016/j.ijmactools.2005.01.028>.
- [19] S.C. Park, M. Chang, Reverse engineering with a structured light system, *Comput. Ind. Eng.* 57 (4) (2009) 1377, <http://dx.doi.org/10.1016/j.cie.2009.07.005>.
- [20] M. Rahrig, M. Torge, 3D inspection of the restoration and conservation of stained glass windows using high resolution structured light scanning, in: The International Archives of the Photogrammetry, Remote Sensing and Spatial Information Sciences, in: Volume XLII-2/W15, 2019 27th CIPA International Symposium Documenting the past for a better future, Ávila, Spain, 2019, pp. 1–5, <http://dx.doi.org/10.5194/isprs-archives-XLII-2-W15-965-2019>.
- [21] Y. Fu, Low-frequency vibration measurement by temporal analysis of projected fringe patterns, *Opt. Las. Eng.* 48 (2010) 226, <http://dx.doi.org/10.1016/j.optlaseng.2009.03.003>.

- [22] R. Rodriguez-Vera, K. Genovese, J.A. Rayas, F. Mendoza-Santoyo, Vibration analysis at microscale by talbot fringe projection method, *Strain* 45 (2009) 249, <http://dx.doi.org/10.1111/j.1475-1305.2008.00611.x>.
- [23] S.T. Yilmaz, U.D. Ozugurel, K. Bulut, M.N. Inci, Vibration amplitude analysis with a single frame using a structured light pattern of a four-core optical fibre, *Opt. Commun.* 249 (4–6) (2005) 515.
- [24] Q. Zhang, X. Su, High-speed optical measurement for the drumhead vibration, *Opt. Express* 13 (8) (2005) 3110.
- [25] M.T. Saita, L.F.G. Dib, E.A. Barbosa, Modeling of structured light projection on vibrating surfaces: Amplitude and phase mapping by fringe visibility evaluation, *Optik* 258 (2022) 168833, <http://dx.doi.org/10.1016/j.ijleo.2022.168833>.
- [26] K. Creath, Phase measurement techniques, in: *Progress in Optics*, Elsevier, 1988, pp. 349–393, [http://dx.doi.org/10.1016/S0079-6638\(08\)70178-1](http://dx.doi.org/10.1016/S0079-6638(08)70178-1).
- [27] B. Gutmann, H. Weber, Phase unwrapping with the branch-cut method: clustering of discontinuity sources and reverse simulated annealing, *Appl. Opt.* 38 (1999) 5577, <http://dx.doi.org/10.1364/ao.38.005577>.
- [28] E.A. Barbosa, A.C.L. Lino, Multiwavelength electronic speckle pattern interferometry for surface shape measurement, *Appl. Opt.* 38 (14) (2007) 2624, <http://dx.doi.org/10.1364/AO.46.002624>.
- [29] D.C. Ghiglia, G.A. Mastin, L.A. Romero, Cellular-automata method for phase unwrapping, *J. Opt. Soc. Amer. A* 4 (1987).